JMEPEG (2005) 14:224-228
DOI: 10.1361/10599490522194

1059-9495/$19.00

Crack Growth in Microalloyed Pipeline Steels for Sour Gas Transport

S. Serna, B. Campillo, and J.L. Albarrán

(Submitted October 8, 2003; in revised form July 23, 2004)

Different cracking modes in a sour gas environment were observed. These modes were mainly related to the microstructure obtained during the manufacturing process of two API X52 microalloyed steels. A banded ferrite/pearlite microstructure was found to be susceptible to hydrogen effects, whereas an acicular ferrite with a grain boundary bainite/bainite microstructure was found to be more susceptible to dissolution in crack-tip regions.

Keywords dissolution, fracture, hydrogen embrittlement, microalloyed steel, microstructure

1. Introduction

The development of microalloyed pipeline steels for applications in the oil field industry for oil and gas transport has been focused on achieving the required yield strength without sacrificing weldability. The addition of niobium (Nb) as a microalloying element in combination with controlled temperature rolling refines the grain size and leads to a banded structure. These procedures improve the strength of the steels (Ref 1), enabling a reduction in the carbon (C) content, leading to improved weldability. Pipeline steels quenched and tempered with additions of vanadium (V) are an alternative for applications in sour gas environments (i.e., those containing hydrogen sulfide, H_2S). Such environments can result in cracking by sulfide stress cracking (SSC) (Ref 2) and hydrogen-induced cracking (HIC) (Ref 3). High-strength microalloyed steels show SSC when a local state of stress is present. Most SSC failures are associated with hydrogen embrittlement (HE) as the main mechanism of cracking, resulting in hydrogen generation on the surface as a product of the H_2S corrosion reaction and permeation into the crack-tip regions (Ref 4). Medium-strength microalloyed steels such as the API X52 grade are more susceptible to HIC in which no external stresses are present (Ref 5). Failures by cracking perpendicular to the rolling direction also have been reported in sour gas environments for medium-strength microalloyed pipeline steels that have hardness values lower than 22 HRC (Ref 6). The present work shows microstructural differences between two API X52 microalloyed pipeline steels, and the crack growth patterns in high H_2S environments at ultimate load conditions to elucidate the mechanisms that induce cracking in these steels.

S. Serna, CIICAP-UAEM, Av. Universidad 1001, 62210 Cuernavaca, Mor., Mexico; **B. Campillo** and **J.L. Albarrán,** Centro de Ciencias Físicas, and Facultad de Química, Universidad Nacional Autónoma de México, P.O. Box 48-3, Cuernavaca, Mor. C.P. 62251, México. Contact e-mail: aserna@uaem.mx.

2. Experimental Procedure

The commercial API X52 pipeline steels used in the present work were supplied in two different conditions: steel X52E was processed by a thermomechanical control process, whereas steel X52T was processed by a quench-and-temper (Q&T) process after hot forming. Samples for microstructural analysis and crack-growth studies were obtained from the microalloyed pipeline steels. Their chemical composition in wt.% is shown in Table 1. For the crack-growth analysis, modified wedge-opening-loading (MWOL) specimens for constant displacement conditions were machined as proposed by Novak and Rolfe (Ref 7) in the longitudinal direction as shown in Fig. 1. The specimens were designed so that they could be manually self-loaded by a bolt. An initial crack was artificially prefatigued to approximately 1.3 mm in length using a mechanical testing machine before loading them to an initial stress-intensity factor, mode I (K_I) value using the back-face strain technique (Ref 8).

The mechanical properties of the microalloyed pipeline steels and MWOL load conditions are given in Table 2. The specimens were assessed for initiation and crack growth at room temperature by immersion in a 150 mL sealed glass vessel containing H_2S-saturated solution A (i.e., sour environment) according to NACE standard TM-0177-99 (Ref 9). Afterward, the specimens were extracted from the vessel, washed in acetone and alcohol, and dried in hot air. The samples were ground, polished, and etched using Nital 2 to develop the crack paths. Microstructural features in the crack-tip regions and fracture surfaces were observed using scanning electron microscopy (SEM) and energy-dispersive x-ray spectroscopy (EDX).

3. Results and Discussion

The microstructure of the API X52 pipeline steel, designated as X52E, is illustrated in Fig. 2(a) and shows uniformly distributed ferrite-pearlite banding in the rolling direction. The ferrite grains show a duplex grain structure that is typical of hot rolled steels followed by rapid cooling (Ref 10). Figure 2(b) corresponds to the X52T steel and shows the presence of acicular ferrite with a carbide phase consisting of fine discrete

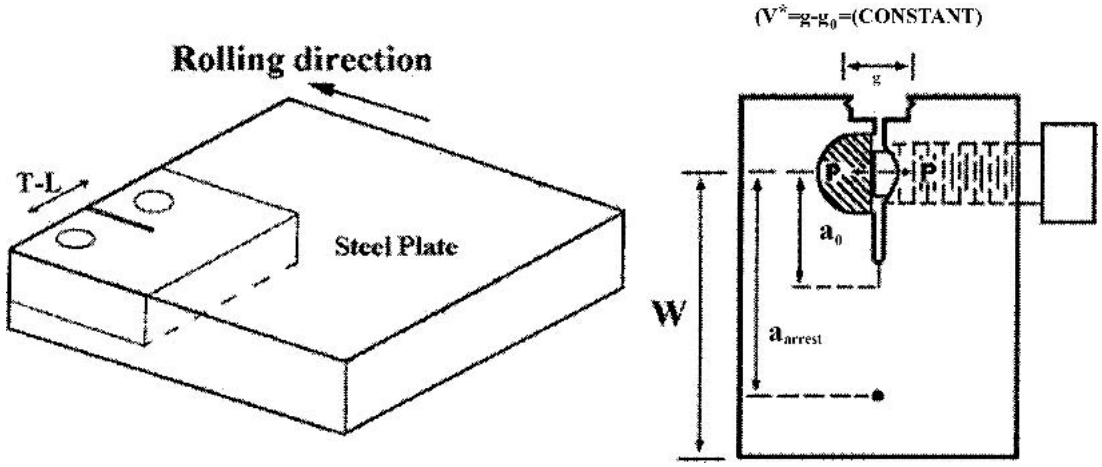

Fig. 1 Specimen orientation and diagram of the MWOL sample: T-L indicates transversal load, W indicates width from applied load point to the end of the sample

Table 1 Chemical composition of API X52 microalloyed pipeline steels

Pipeline steel	Chemical composition, wt.%												
	C	Si	Mn	P	S	Al	Cu	Ni	Cr	Mo	V	Nb	Ti
X52E	0.06	0.30	1.05	0.013	0.002	…	0.25	0.02	0.02	0.008	0.05	0.05	0.02
X52T	0.075	0.334	0.823	0.013	0.003	0.021	0.126	0.043	0.033	…	0.031	…	0.014

Table 2 Mechanical properties and load conditions for API X52 microalloyed pipeline steels

Pipeline steel	Rockwell B hardness, HRB	Yield strength (YS), MPa	Ultimate tensile strength (UTS), MPa	Total strain, %	Stress-intensity factor (K_I), MPa$\sqrt{m}$	Crack-opening displacement (COD), mm
X52E	91	382	470	26	43.48	0.359
X52T	87	343	453	42	39.58	0.354

carbides and small patches of tempered pearlite and/or bainite, preferentially segregated at the grain boundaries.

Figure 3 shows cracks parallel to the rolling direction of the pipeline steels that propagate perpendicular to the stress direction. Crack length in the X52E steel was greater than that in the X52T steel (Fig. 3a). In the X52T steel, crack growth was more irregular and noncontinuous (Fig. 3b). By analyzing the crack-tip zones illustrated by Fig. 4, the differences in the microstructure induce different mechanisms for cracking. In Fig. 4(a), the X52E steel did not show any appreciable dissolution zones. Instead, a significant amount of microcracking occurs in front of the crack (i.e., the zone indicated by the arrow in Fig. 3a). The microcracks observed there were formed by void coalescence at the grain boundaries. This is indicated by the arrows in the figure. Additionally, the pearlite grains deflect the crack into the softer ferrite. Also, the inclusions play an important role by trapping evolved hydrogen at the crack tip. On the other hand, steel X52T show dissolution "bulbs" at approximately 45° to the advancing crack (Fig. 4b). This cracking mechanism can be attributed to the Q&T process that induces lower strain hardening, promoting the mobility of defects that could trap additional hydrogen at the crack tip. The corrosion products detected by EDX within the crack tip were Fe(O, S) compounds.

The basic corrosion reaction, taking place between the steel and H_2S, generates hydrogen. Although the dissolution exhibited in the crack tip of the X52E steel is small, in comparison with the dissolution observed in the fracture surface exposed to the solution (Fig. 6), it generates enough hydrogen to cause damage. A fraction can be absorbed at the crack tip and trapped into the plastic zone ahead of the crack tip generating microcracks following a mainly transgranular path. Several reports have been published elsewhere (Ref 11, 12) regarding metal dissolution and HE in other microalloyed steels in sour environments.

In relation to X52T steel, the morphology of the crack tip indicates that the crack-growth mechanism is due to slip dissolution. Crack growth occurs in a cycle of extremely localized anodic dissolution combined with the fracture of a protective film due to plastic strain (Ref 13, 14). An EDX pattern taken inside one of the dissolution bulbs (Fig. 4b, insert) indicates that an Fe(O, S) film forms inside the crack and can be fractured as a result of the applied stress.

The banded microstructure of the X52E steel is more susceptible to hydrogen, as shown by the appearance of small cracks (i.e., microcracking) in front of the crack tip. This effect can be related to the higher concentration of precipitates such as carbides or carbonitrides of Nb, titanium (Ti), and V, which

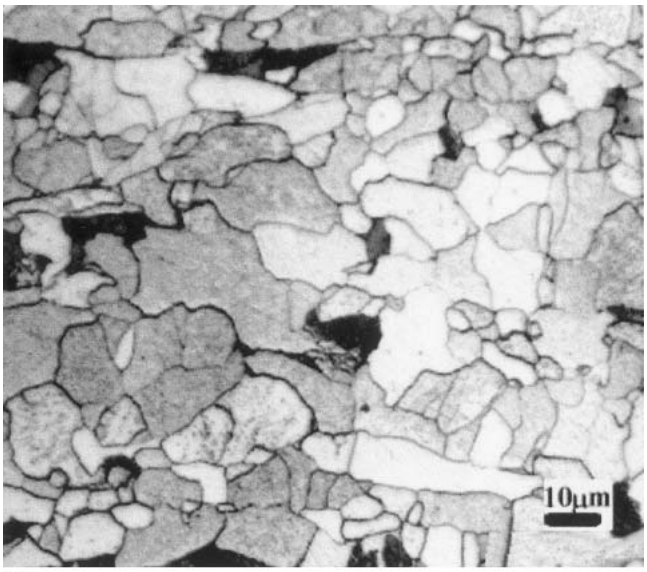

(a)

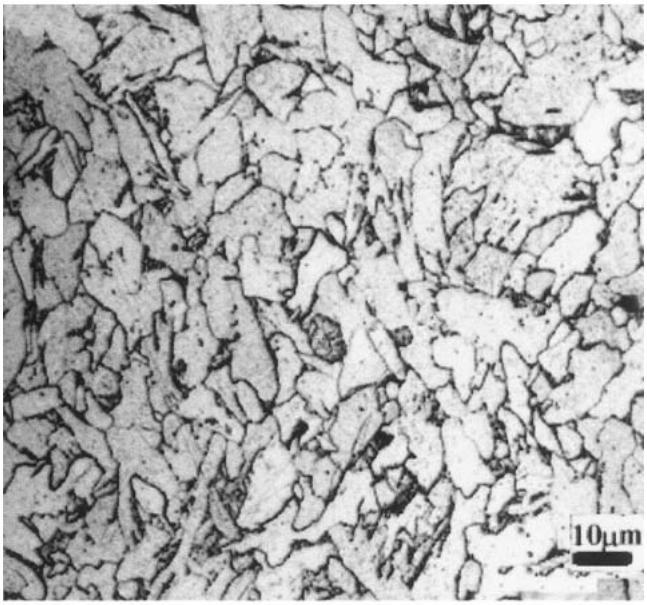

(b)

Fig. 2 Steels microstructure. (a) X52E. (b) X52T

are preferentially located at the grain boundaries. Also, these elements are hydride formers, so they can fracture in a brittle manner in the crack-tip plastic zone, further enhancing microcrack formation (Fig. 4a). Furthermore, this steel is well within the hardness level specified by NACE standard MR0175-92 (Ref 6) that is required for safe performance in sour gas environments. Hence, it may be possible that microcracking also can be related to, or complemented by, another mechanism, such as hydrogen-enhanced local plasticity (Ref 4). Further evidence is needed, however, to show that this mechanism may be active.

Regarding the X52T steel, the crack front intersects the aforementioned microstructure of acicular ferrite and small patches of pearlite and/or bainite at grain boundaries (Fig. 2b). Thus, this type of microstructure, in conjunction with the sour gas environment, can lead to the creation of electrochemical microcells that contribute to dissolution. In addition, the tempering treatment leads to a more uniform distribution of precipitates, mainly carbides based on V and Ti, allowing hydrogen to be trapped, thereby decreasing its overall effect on cracking. This process has been recognized in chromium-molybdenum (Cr-Mo) steels and also in V microalloyed steelsin the quenched-and-tempered condition (Ref 15).

Figure 5 shows crack growth as a function of testing time. It can be seen that the overall curve for steel X52T, including the dashed zone, has a smaller crack length than steel X52E. This agrees with results previously reported for larger crack-growth rates when hydrogen is involved in crack growth, as seen in the X52E steel (Ref 16). The fracture surfaces obtained from the two steels are shown in Fig. 6, and two different crack-paths were observed. One path is curved and corresponds to the X52T steel. It is characterized by ductile fracture. For steel X52E, the path is almost planar and corresponds to brittle fracture. This is in agreement with cracking modes in microalloyed pipeline steels. The crack length in the fracture surface of steel X52T (Fig. 6) was about 13.2 mm. This was measured between points 1 and 2, where point 2 corresponds in Fig. 2(b) to the point indicated by the arrow and is indicated in Fig. 5 as the beginning of the dashed line. The rest of the crack corresponds to dissolution bulbs at surface level along the axial load axis, with the dashed line in Fig. 5 indicating the behavior observed on the surface. It is important to point out that the crack tip seen in Fig. 4(b) was taken from the region indicated by the arrow in Fig. 3(b).

These results indicate that differences in the microstructure as a result of the thermomechanical process route affects cracking behavior in sour gas environments. Analysis indicates that the X52T steel microstructure is more suitable for this application. Recently, similar results have been obtained in a homogeneous Q&T bainite/martensite microstructure compared with rolled and normalized ferritic-pearlitic microstructures (Ref 17).

4. Conclusions

Different thermomechanical processes produced two microalloyed pipeline steels of grade API X52. The microstructure formed during manufacturing can alter the cracking mode from one of pure dissolution for acicular ferrite to SSC associated with HE for banded ferrite/pearlite. A key factor that decreases the effect of hydrogen on cracking is the uniform distribution of precipitates, mainly V and Ti carbides that are present at the grain boundaries in the X52T steel. This situation leads to lower crack-growth rates, thus improving the cracking resistance of this steel.

Acknowledgments

The support provided by the Instituto Mexicano del Petróleo under project D.00041 (Programa de Investigación y Desarrollo de Ductos) is greatly appreciated, and special thanks are due to Dr. M. Amaya. Also, the authors wish to acknowledge the technical support provided by O. Flores and A. Gonzalez.

References

1. Y. Kobayashi, Recent High Performance Line Pipe for Oil/Gas Production, *Proc. VIII Seminar Mexico-Japan '94,* K. Kawakami, Ed., JICA, Mexico City, 1994, p 9-1 to 9-12
2. H. Asahi, M. Ueneo, and T. Yonezawa, Prediction of Sulfide Stress

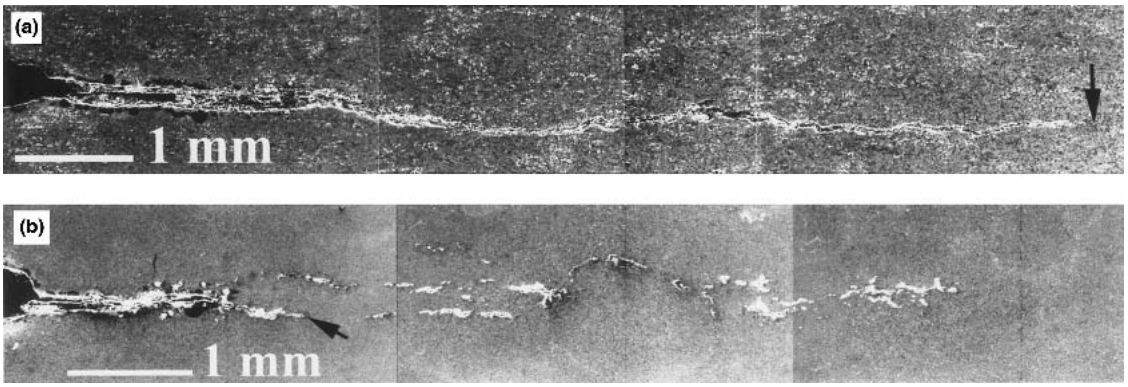

Fig. 3 Crack lengths obtained after exposure of steels to a sour environment. (a) X52E. (b) X52T

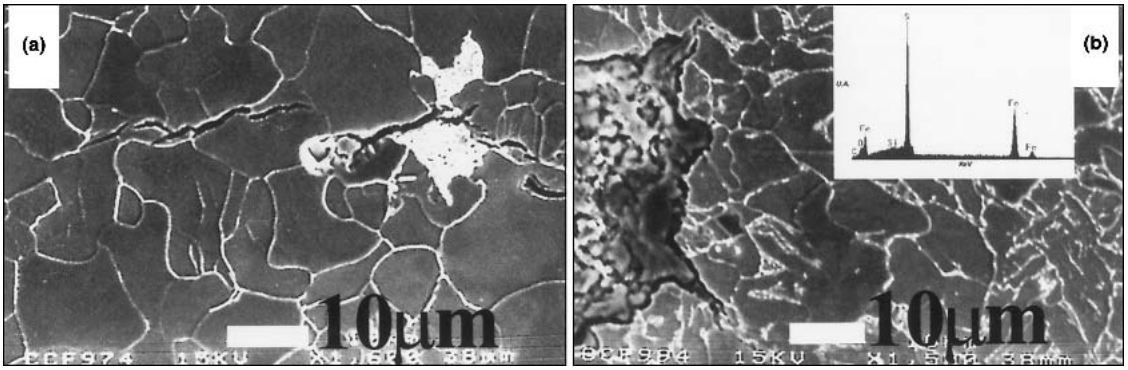

Fig. 4 Crack tips (a) X52E and (b) X52T, with EDX of corrosion products

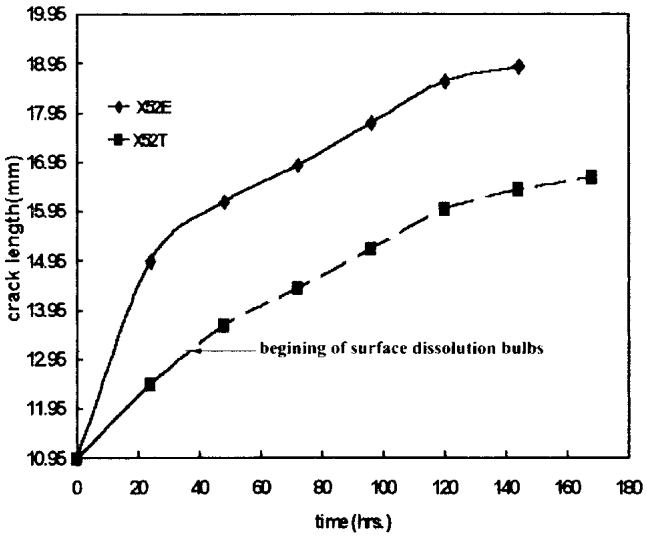

Fig. 5 Crack length versus time of both steels and the plot for steel X52T shows a dashed zone that indicates a superficial crack growth

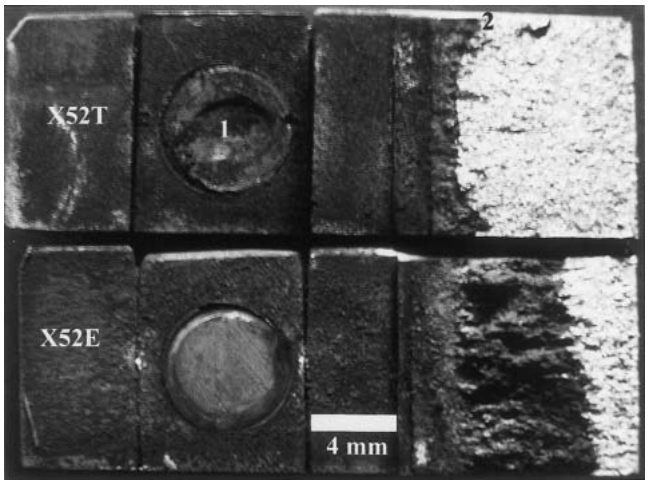

Fig. 6 Steel fracture surfaces, showing different crack paths. The number "2" over the X52T steel fracture indicates the start of the surface dissolution bulbs.

Cracking in High Strength Tubulars, *Corrosion,* Vol 50 (No. 7), 1994, p 537-545

3. G.M. Pressouyre, R.T. Blondeau, G. Primon, and L. Cadiou, Very Low Inclusion and Impurity Content Steels as a Solution to Resist Sour Environments, *Proc. First Int. Conf. Current Solutions to Hydrogen Problems in Steels,* C.G. Interrater and G.M. Pressouyre, Ed., ASM International, 1982, p 212-221
4. H.K. Birnbaum, Mechanisms of Hydrogen-Related Fracture of Metals, *Environment-Induced Cracking of Metals,* R.P. Gangloff and M.B. Ives, Ed., National Association of Corrosion Engineers (NACE) International, 1990, p 21-29
5. B. Craig, Limitations of Alloying to Improve the Threshold for Hydrogen Stress Cracking of Steel, *Hydrogen Effects on Material Behavior,* N.R. Moody and A.W. Thompson, Ed., TMS-AIME, 1990, p 955-963
6. "Sulfide Stress Cracking Resistant Metallic Materials for Oilfield Equipment," Standard MR0175-99, NACE International, 1999
7. S.R. Novak and S.T. Rolfe, Modified WOL Specimen for K_{Iscc} Environmental Testing, *J. of Materials,* Vol 4 (No. 3), 1969, p 701-728
8. W.F. Deans and C.E. Richards, A Simple and Sensitive Method of

Monitoring Crack and Load in Compact Fracture Mechanics Specimens Using Strain Gages, *J. Test. Eval.,* Vol 7, 1979, p 147-154
9. "Laboratory Testing of Metals for Resistance to Specific Forms of Environmental Cracking in H2S Environments," Standard TM-0177-99, NACE International, 1999
10. J.Q. Wang, A. Atrens, D.R. Cousens, and N. Kinaev, Microstructure of X52 and X65 Pipeline Steels, *J. Mater. Sci.,* Vol 34, 1999, p 1721-1728
11. F.P. Ford, Environmental Induced Cracking: The Interaction Between Mechanism and Design, *Corrosion/86: Symposium on Environmental Cracking-The Interactions Between Mechanisms and Design,* NACE International, 1986, p 113
12. J.L. Albarrán, L. Martínez, and H.F. López, The Sour Gas Susceptibility of an X-80 Steel for Oil and Gas Transport, *Scr. Mater.,* Vol 38 (No. 5), 1998, p 751-752
13. D.A. Vermilyea, A Film Rupture Model for Stress Corrosion Cracking, *Stress-Corrosion Cracking and Hydrogen Embrittlement of Iron-Base Alloys,* R.W. Staehle, J. Hochmann, R.D. McCright, and J.E. Slater, Ed., National Association of Corrosion Engineers, 1977, p 208-217
14. R.W. Staehle, Predictions and Experimental Verifications of the Slip Dissolution Model for Stress Corrosion Cracking of Low Strength Alloys, *Stress-Corrosion Cracking and Hydrogen Embrittlement of Iron-Base Alloys,* R.W. Staehle, J. Hochmann, R.D. McCright, and J.E. Slater, Ed., National Association of Corrosion Engineers, 1977, p 180-207
15. E. Anelli, L. Cariboni, and A. Mascanzoni, Analysis of Metallurgical Factors Controlling the SSCC Resistance of Quenched and Tempered Microalloyed Steels, *Processing, Microstructure and Properties of HSLA Steels,* A.J. DeArdo, Ed., TMS, 1988, p 477-495
16. T. Boellinghaus and H. Hoffmeister, Numerical Model for Hydrogen-Assisted Cracking, *Corrosion,* Vol 56 (No. 6), 2000, p 611-614
17. R.A. Carneiro, R.C. Ratnapuli, and V. de Freitas Cunha Lins, The Influence of Chemical Composition and Microstructure of API Linepipe Steels on Hydrogen Induced Cracking and Sulfide Stress Corrosion Cracking, *Mater. Sci. Eng., A,* Vol 357, 2003, p 104-110